JOURNAL OF GUIDANCE, CONTROL, AND DYNAMICS
Vol. 34, No. 1, January–February 2011

Coulomb Control of Nonequilibrium Fixed Shape Triangular Three-Vehicle Cluster

Shuquan Wang* and Hanspeter Schaub†
University of Colorado, Boulder, Colorado 80309

DOI: 10.2514/1.47835

This paper studies a three-body Coulomb virtual structure control problem. For a formation of three spacecraft flying freely in deep space, actively controlled Coulomb forces are used to stabilize the formation to a shape-fixed triangular configuration. The control problem is challenging because the system is nonlinear and nonaffine, while the direct control of all three sides at the same time is often not implementable using only real charges. Firstly, a two-side switched control strategy is developed to control the two sides with the worst shape errors such that the implementable charge control solution is guaranteed. However, analytical and practical stability issues arise due to the discrete control time steps. Using the multiple Lyapunov functions analysis tool, a stable switched control strategy is set up in a manner such that the activated error function is decreasing rapidly enough to compensate for a potentially increased amount during the last uncontrolled control cycle. Thus all the error functions are made Lyapunov-like and the global stability of the switched control strategy is guaranteed. Perfect convergence to desired triangular shape is not physically achievable with Coulomb forces alone because the general triangular shape is not a natural equilibrium solution. Numerical simulations illustrate the effectiveness of the stable switched control strategy.

I. Introduction

A SPACECRAFT virtual structure is a cluster or formation of spacecraft with a fixed relative configuration forming a desired shape to satisfy mission sensor requirements. A feedback control strategy is required to stabilize the spacecraft to the reference configuration. The goal is to be able to place sensors at desired locations to provide the required baselines to satisfy mission objectives. The free-flying concept is attractive in that it allows for large sensor baselines to be considered, and the overall cluster shape can be changed over time to accommodate changing mission sensing requirements. The virtual structure approach is a convenient method to prescribe a coordinated behavior of the formation because this approach assumes the reference structure fixed in the Hill frame. Reference [1] develops a formation feedback control strategy to achieve the virtual structure control. The authors at first assume that a rigid structure is in orbit, then use an inverse dynamics method to determine a feedforward reference control using thrusters that can maintain the spacecraft in the rigid structure configuration. At last a feedback control loop is used to stabilize the spacecraft cluster about the virtual structure. This virtual structure control is based on the thrusters' capability to control the three-dimensional motions of the satellites.

In contrast, this paper studies a Coulomb virtual structure control problem. As compared with the traditional virtual structure control, Coulomb virtual structure control is a very different problem because the direct controllability of the relative satellite positions is not present. A Coulomb virtual structure uses only electrostatic forces (Coulomb forces) to control the shape of the formation, and not necessarily the formation's inertial position and orientation. The use of Coulomb forces to control spacecraft relative motion was first investigated by King et. al. in 2002 [2]. Since then many applications of the Coulomb formation flying (CFF) concept have been studied. These include CFF equilibrium solutions [3–6], two-craft Coulomb tether control [7–10], hybrid propulsion strategy combining Coulomb forces and electric thrusters [11], as well as spacecraft collision avoidance using Coulomb forces [12–14]. Considering the plasma environment in space, the Coulomb thrusting approach is applicable in tight clustered space missions in geostationary orbits (GEOs) or in deep space where the Debye shielding effect is not very strong and the separation distances are within 100 m.

The studies of open-loop equilibrium charge solutions and Coulomb virtual tether control are related to Coulomb virtual structure control, but they focus on different aspects. The Coulomb tether papers present the first examples of feedback stabilized virtual Coulomb structures [7–10]. However, their control methodology does not scale to systems with more than two spacecraft. References [15–17] are more closely related to the Coulomb virtual structure control problem considered in this paper. Reference [15] studies constant charge invariant shape solutions for spinning three-craft Coulomb formation. It shows that only the collinear configuration and expanding equilateral triangle configuration can be invariant assuming a fixed spacecraft potential. Reference [16] introduces the spinning two-craft Coulomb tether concept. It is the first work that analyzes the open-loop stability of a Coulomb tether with constant spacecraft charges, based on a linearized model. Assuming the Coulomb tether flying in deep space, it shows that the radial motion is locally stable if the spacecraft separation distance is less then the Debye length. Reference [17] studies the three-craft Coulomb tether problem. Based on a linearized model about a collinear equilibrium configuration, a linear feedback control is developed to stabilize the Coulomb tether to the collinear relative equilibria. The nonlinear system converges to a neighborhood of the desired equilibrium, but due to the approximation using linearization technique, the size of the convergence neighborhood is limited. General triangular formation shapes, or nonequilibrium collinear shapes, are not feasible with this control strategy.

The three-craft Coulomb virtual structure control is a good start to the general N-craft Coulomb virtual structure problem. Reference [18] studies a one-dimensionally constrained three-craft Coulomb virtual structure control. Here a two stage control strategy is developed to make the one-dimensional three-craft formation converge to a desired configuration. The first stage uses saturated control to stabilize the relative motion of the formation. After the relative motion is stabilized, the second stage is engaged to control the shape of the formation to converge to the desired shape. The control convergence domains are found numerically. But for a

Received 26 October 2009; revision received 23 June 2010; accepted for publication 20 August 2010.

*Graduate Research Assistant, Aerospace Engineering Sciences Department; shuquan.wang@colorado.edu. Student Member AIAA.

†Associate Professor and H. Joseph Smead Fellow, Aerospace Engineering Sciences Department. Associate Fellow AIAA.

symmetric configuration case, analytical criterion is derived analytically. The one-dimensional nature of this work allows for significant mathematical simplifications, and provides for a dynamic system where solving for the charge products always leads to real and unique individual charge solutions.

This paper extends the work in [18] into three-dimensional space. This extension results in a significant increase in the complexity of the dynamic system, as well as the control implementation. While the products of the spacecraft charges appear linearly in the dynamics, the mapping to individual charges can yield imaginary solutions at times. Thus a standard inverse dynamics solution is not feasible here. Instead, a Lyapunov-based nonlinear control strategy is sought which stabilizes the configuration of the three-craft formation to an arbitrary triangular shape. This paper studies how to develop an implementable control strategy while still ensuring the stability of the system. One method to guarantee an implementable control is to always control the worst two sides of the triangle. However, such switching strategy can cause stability issues due to the discrete control time steps. Multiple Lyapunov functions analysis is a tool to analyze the stability of a switched system. This paper investigates how to modify the switched control strategy such that the stability of the charged spacecraft virtual structure system is ensured. Because the general triangular shape (except for the collinear configuration case) does not have an equilibrium charge solution, the asymptotic stability is not achievable. Numerical simulations illustrate the closed-loop performance of the new three-craft charge control strategy.

This paper makes several simplifications to investigate the control of a triangular configuration of a Coulomb virtual structure. This work is the first step into the Coulomb virtual control in real situation, in which the gravitational forces, Debye shielding, etc., are considered. The control problem gets complicated fast when the discrete control input is considered. The influences of the gravitational forces and Debye shielding are beyond the scope of this paper and are the next step to the Coulomb virtual control problem.

II. Separation Distance Equations of Motion

This paper considers a three-spacecraft cluster flying in the three-dimensional free space where there are no external forces acting on the system. The scenario of the three-body Coulomb virtual structure is shown in Fig. 1. Assuming point-charge models for the spacecraft, the Coulomb force between the ith and jth spacecraft exerted by the ith spacecraft is given by [14]

$$\boldsymbol{F}_{ij} = -k_c \frac{q_i q_j}{r_{ij}^2}\left(1 + \frac{r_{ij}}{\lambda_d}\right)\exp\left(-\frac{r_{ij}}{\lambda_d}\right)\hat{e}_{ij} \tag{1}$$

where $k_c = 8.99 \times 10^9\ \mathrm{Nm^2\,C^{-2}}$ is the Coulomb constant, q_i is the charge of the ith spacecraft which can be actively controlled, $r_{ij} = \|\boldsymbol{r}_{ij}\|$ is the separation distance between the ith and jth spacecraft, $\hat{\boldsymbol{e}}_{ij}$ is the unit vector pointing from the ith to jth spacecraft. The parameter λ_d is the Debye length which characterizes the plasma shielding effect. It is influenced by the temperature and the ion/electron density. The Debye length ranges within $[0.02, 0.4]$ m in low Earth orbit, $[142, 1496]$ m in GEO and $[20, 40]$ m at 1 astronomical unit in deep space [2]. Generally it is assumed that the Coulomb thrusting is applicable only when the separation distance is less than the local Debye length. In developing the control algorithm, it is assumed that $\lambda_d = \infty$ which indicates that the plasma shielding effect is not explicitly considered.

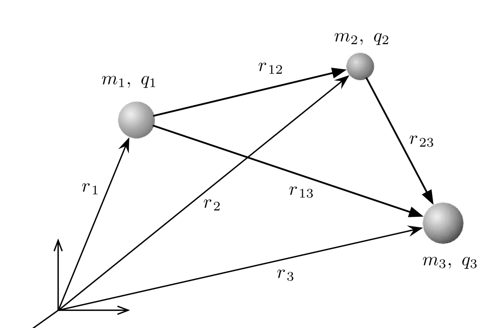

Fig. 1 Scenario of the three-body system.

By the assumption that there are no external forces acting on the three-body system, the inertial equations of motion (EOMs) are given by

$$m_1\ddot{\boldsymbol{r}}_1 = -k_c\frac{q_1q_2}{r_{12}^2}\hat{\boldsymbol{e}}_{12} - k_c\frac{q_1q_3}{r_{13}^2}\hat{\boldsymbol{e}}_{13} \tag{2a}$$

$$m_2\ddot{\boldsymbol{r}}_2 = k_c\frac{q_1q_2}{r_{12}^2}\hat{\boldsymbol{e}}_{12} - k_c\frac{q_2q_3}{r_{23}^2}\hat{\boldsymbol{e}}_{23} \tag{2b}$$

$$m_3\ddot{\boldsymbol{r}}_3 = k_c\frac{q_1q_3}{r_{13}^2}\hat{\boldsymbol{e}}_{13} + k_c\frac{q_2q_3}{r_{23}^2}\hat{\boldsymbol{e}}_{23} \tag{2c}$$

where m_i is the mass of the ith spacecraft, $\boldsymbol{r}_i$ is the inertial position of the ith spacecraft.

This paper intends to develop a control algorithm to make the three-body formation assume a certain desired shape. The shape of a three-body formation can be completely defined by the three separation distances between any two spacecraft. Mathematically, the objective of the control to be making the three separation distances $(r_{12}, r_{23}, r_{13})^T$ converge to the desired distances $(r_{12}^*, r_{23}^*, r_{13}^*)^T$. The first step is to identify the separation distances' EOMs.

For the notational convenience, a vector $\boldsymbol{\xi}$ is defined as a function of the charge products:

$$\boldsymbol{\xi} = (\xi_1, \xi_2, \xi_3)^T = \left(k_c\frac{q_1q_2}{r_{12}^2}, k_c\frac{q_2q_3}{r_{23}^2}, k_c\frac{q_1q_3}{r_{13}^2}\right)^T \tag{3}$$

Based on the inertial EOM in Eq. (2), the relative positions' EOMs are found:

$$\ddot{\boldsymbol{r}}_{12} = \ddot{\boldsymbol{r}}_2 - \ddot{\boldsymbol{r}}_1 = \xi_1\left(\frac{1}{m_1} + \frac{1}{m_2}\right)\hat{\boldsymbol{e}}_{12} - \xi_2\frac{1}{m_2}\hat{\boldsymbol{e}}_{23} + \xi_3\frac{1}{m_1}\hat{\boldsymbol{e}}_{13} \tag{4a}$$

$$\ddot{\boldsymbol{r}}_{23} = \ddot{\boldsymbol{r}}_3 - \ddot{\boldsymbol{r}}_2 = -\xi_1\frac{1}{m_2}\hat{\boldsymbol{e}}_{12} + \xi_2\left(\frac{1}{m_2} + \frac{1}{m_3}\right)\hat{\boldsymbol{e}}_{23} + \xi_3\frac{1}{m_3}\hat{\boldsymbol{e}}_{13} \tag{4b}$$

$$\ddot{\boldsymbol{r}}_{13} = \ddot{\boldsymbol{r}}_3 - \ddot{\boldsymbol{r}}_1 = \xi_1\frac{1}{m_1}\hat{\boldsymbol{e}}_{12} + \xi_2\frac{1}{m_3}\hat{\boldsymbol{e}}_{23} + \xi_3\left(\frac{1}{m_1} + \frac{1}{m_3}\right)\hat{\boldsymbol{e}}_{13} \tag{4c}$$

The relationship between the separation distance's acceleration $\ddot{r}_{ij}$ and the relative acceleration $\ddot{\boldsymbol{r}}_{ij}$ is achieved by differentiating the identity $r_{ij} = \sqrt{\boldsymbol{r}_{ij}\cdot\boldsymbol{r}_{ij}}$ twice:

$$\ddot{r}_{ij} = \ddot{\boldsymbol{r}}_{ij}\cdot\hat{\boldsymbol{e}}_{ij} + \frac{1}{r_{ij}}\|\dot{\boldsymbol{r}}_{ij}\|^2(1 - \cos^2\angle(\boldsymbol{r}_{ij}, \dot{\boldsymbol{r}}_{ij})) \tag{5}$$

where $\angle(\boldsymbol{r}_{ij}, \dot{\boldsymbol{r}}_{ij})$ denotes the angle between the two vectors $\boldsymbol{r}_{ij}$ and $\dot{\boldsymbol{r}}_{ij}$.

Substituting the relative positions' EOMs in Eq. (4) into Eq. (5), yields the separation distances' EOMs:

$$\ddot{r}_{12} = \xi_1\left(\frac{1}{m_1} + \frac{1}{m_2}\right) + \xi_2\frac{1}{m_2}\cos\alpha_2 + \xi_3\frac{1}{m_1}\cos\alpha_1 + f_1 \tag{6a}$$

$$\ddot{r}_{23} = \xi_1\frac{1}{m_2}\cos\alpha_2 + \xi_2\left(\frac{1}{m_2} + \frac{1}{m_3}\right) + \xi_3\frac{1}{m_3}\cos\alpha_3 + f_2 \tag{6b}$$

$$\ddot{r}_{13} = \xi_1\frac{1}{m_1}\cos\alpha_1 + \xi_2\frac{1}{m_3}\cos\alpha_3 + \xi_3\left(\frac{1}{m_1} + \frac{1}{m_3}\right) + f_3 \tag{6c}$$

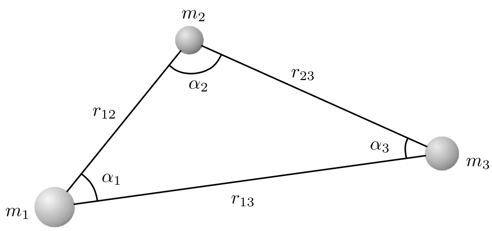

Fig. 2 Geometry of the three-body system.

where α_i is the angle of the two sides cornered at the ith spacecraft as shown in Fig. 2, f_i is given by

$$f_1 = \|\dot{\boldsymbol{r}}_{12}\|(1 - \cos^2\angle(\boldsymbol{r}_{12}, \dot{\boldsymbol{r}}_{12})) \tag{7a}$$

$$f_2 = \|\dot{\boldsymbol{r}}_{23}\|^2(1 - \cos^2\angle(\boldsymbol{r}_{23}, \dot{\boldsymbol{r}}_{23})) \tag{7b}$$

$$f_3 = \|\dot{\boldsymbol{r}}_{13}\|^2(1 - \cos^2\angle(\boldsymbol{r}_{13}, \dot{\boldsymbol{r}}_{13})) \tag{7c}$$

III. Virtual Structure Control Strategy

The objective of the Coulomb virtual structure control is to stabilize the cluster to the desired triangle. The inertial orientation is not concerned. Mathematically the goal of the control is to make the separation distances converge to the given desired distances:

$$(r_{12}, r_{23}, r_{13})^T \rightarrow (r_{12}^*, r_{23}^*, r_{13}^*)^T \tag{8}$$

This paper assumes that the desired shape of the three-body system is stationary, which means that the three separation distances are constant. Using the state vector $\boldsymbol{X} = (r_{12}, r_{23}, r_{13})^T$, the separation distances' EOMs in Eq. (6) are rewritten into a concise form as

$$\ddot{\boldsymbol{X}} = [B]\boldsymbol{\xi} + \boldsymbol{f} \tag{9}$$

where $\boldsymbol{f} = (f_1, f_2, f_3)^T$, and the matrix $[B]$ is

$$[B] = \begin{bmatrix} \left(\frac{1}{m_1} + \frac{1}{m_2}\right) & \frac{\cos\alpha_2}{m_2} & \frac{\cos\alpha_1}{m_1} \\ \frac{\cos\alpha_2}{m_2} & \left(\frac{1}{m_2} + \frac{1}{m_3}\right) & \frac{\cos\alpha_3}{m_3} \\ \frac{\cos\alpha_1}{m_1} & \frac{\cos\alpha_3}{m_3} & \left(\frac{1}{m_1} + \frac{1}{m_3}\right) \end{bmatrix} \tag{10}$$

Define the state tracking error to be

$$\Delta\boldsymbol{X} = \boldsymbol{X} - \boldsymbol{X}^* \tag{11}$$

where $\boldsymbol{X}^* = (r_{12}^*, r_{23}^*, r_{13}^*)^T$ is the array of desired separation distances.

The objective of the control is to find an implementable solution of $\boldsymbol{\xi}$ to make $\Delta\boldsymbol{X} \rightarrow 0$. Note that $\boldsymbol{\xi}$ is a linear function of the charge products. But the individual charges of spacecraft are the ultimate control inputs of the control system, which makes this a nonaffine control problem. Not all the combinations of the charge products result in real solutions of individual charges, some combinations result in complex values of individual charges. Those complex solutions of individual charges are not physically implementable. This issue will be discussed and addressed later on.

A. Three-Side Control Law

First, let us consider the case where all three sides are to be controlled at once. As will be seen, this three-side control solution does not always result in real charge solutions due to the nonaffine nature of the Coulomb forces. Let us define a Lyapunov function candidate as

$$V = \frac{1}{2}\Delta\boldsymbol{X}^T[K]\Delta\boldsymbol{X} + \frac{1}{2}\Delta\dot{\boldsymbol{X}}^T\Delta\dot{\boldsymbol{X}} \tag{12}$$

where $[K]$ is a 3×3 positive definite matrix. Let us use $[K] = k[I_{3\times3}]$ for simplicity with $k > 0$ being constant. Taking a first-order time derivative of V and using the EOMs in Eq. (9), yields

$$\dot{V} = \Delta\dot{\boldsymbol{X}}^T([K]\Delta\boldsymbol{X} + \Delta\ddot{\boldsymbol{X}}) = \Delta\dot{\boldsymbol{X}}^T([K]\Delta\boldsymbol{X} + [B]\boldsymbol{\xi} + \boldsymbol{f}) \tag{13}$$

To guarantee overall stability set $\dot{V}$ to be a negative semidefinite function

$$\dot{V} = -\Delta\dot{\boldsymbol{X}}^T[P]\Delta\dot{\boldsymbol{X}} \tag{14}$$

where $[P]$ is a 3×3 positive definite matrix. Note that this form of $\dot{V}$ is negative semidefinite, not negative definite. This is because V is a function of both $\Delta\boldsymbol{X}$ and $\Delta\dot{\boldsymbol{X}}$, but $\dot{V}$ is only explicitly a function of only $\Delta\dot{\boldsymbol{X}}$.

Substituting Eq. (14) into Eq. (13) and solving for $\boldsymbol{\xi}$, yields

$$\boldsymbol{\xi} = [B]^{-1}(-[K]\Delta\boldsymbol{X} - \boldsymbol{f} - [P]\Delta\dot{\boldsymbol{X}}) \tag{15}$$

Note that even though $\dot{V}$ is negative semidefinite, the control law given by Eq. (15) is driving the state tracking error $\Delta\boldsymbol{X}$ converge to zero. This can be proved by the following two steps. The second-order time derivative of V is

$$\ddot{V} = -2\Delta\dot{\boldsymbol{X}}^T[P]\Delta\ddot{\boldsymbol{X}} \tag{16}$$

When $\dot{V} = 0$ which indicates $\Delta\dot{\boldsymbol{X}}$, $\ddot{V} = 0$. Taking a third-order time derivative of V

$$\dddot{V} = -2\Delta\ddot{\boldsymbol{X}}^T[P]\Delta\ddot{\boldsymbol{X}} - 2\Delta\dot{\boldsymbol{X}}^T[P]\Delta\dddot{X} \tag{17}$$

When $\dot{V} = 0$, it is obvious that $\dddot{V} \leq 0$ and $\dddot{V} = 0$ only when $\Delta\boldsymbol{X} = 0$. Thus the system is asymptotically stable if the control law given by Eq. (15) can be implemented.

From the definition of $\boldsymbol{\xi}$ in Eq. (3), the individual charges are solved through

$$\begin{cases} q_1 = \sqrt{\frac{\xi_1\xi_3}{\xi_2 k_c}\frac{|r_{12}r_{13}|}{|r_{23}|}} \\ q_2 = \mathrm{sign}(\xi_2\xi_3)\sqrt{\frac{\xi_1\xi_2}{\xi_3 k_c}\frac{|r_{12}r_{23}|}{|r_{13}|}} \\ q_3 = \mathrm{sign}(\xi_3)\sqrt{\frac{\xi_2\xi_3}{\xi_1 k_c}\frac{|r_{23}r_{13}|}{|r_{12}|}} \end{cases} \tag{18}$$

Notice that Eq. (18) does not necessarily result in real solutions of the individual charges. If $\xi_1 \cdot \xi_2 \cdot \xi_3 < 0$, the individual charges are imaginary and are not physically implementable. By the definition in Eq. (3), $\xi_1 \cdot \xi_2 \cdot \xi_3 \propto (q_1 q_2 q_3)^2$. For an implementable solution of $\boldsymbol{\xi}$, the following inequality must be satisfied:

$$\xi_1 \cdot \xi_2 \cdot \xi_3 \geq 0 \tag{19}$$

However, the inequality in Eq. (19) is not guaranteed from the three-side control algorithm in Eq. (15). Some special strategy has to be engaged to make the control algorithm physically implementable.

B. Two-Side Control Switch Strategy

The previous section develops a Lyapunov-based control law that controls the three triangle side-lengths at once. The control is asymptotically stable, but it is not always physically implementable because at times it requires imaginary charges. If we control two sides at once instead of controlling three sides, correspondingly a subset of the state-space EOMs in Eq. (9) are considered, then the control input matrix $[B]$ becomes a 2×3 matrix. Using the null space of the control input matrix, there is a family of solutions that have the same response. An implementable solution can always be found out from this solution family. The use of the null space of the input matrix to determine implementable real charge solutions is discussed in [18].

This paper proposes a strategy that always controls the worst two sides of the triangle. By continuously switching to control the worst two sides, it is expected that the system is stabilized and the state tracking error converge to zero. However, the actual switching strategy must be carefully chosen to avoid making the system unstable. This paper defines the switching criterion by investigating the three sub-Lyapunov functions:

$$V_a = \frac{1}{2}k(\Delta X_1^2 + \Delta X_3^2) + \frac{1}{2}(\Delta \dot{X}_1^2 + \Delta \dot{X}_3^2) \triangleq \frac{k}{2}\Delta \boldsymbol{X}_a^T \Delta \boldsymbol{X}_a + \frac{1}{2}\Delta \dot{\boldsymbol{X}}_a^T \Delta \dot{\boldsymbol{X}}_a \tag{20a}$$

$$V_b = \frac{1}{2}k(\Delta X_1^2 + \Delta X_2^2) + \frac{1}{2}(\Delta \dot{X}_1^2 + \Delta \dot{X}_2^2) \triangleq \frac{k}{2}\Delta \boldsymbol{X}_b^T \Delta \boldsymbol{X}_b + \frac{1}{2}\Delta \dot{\boldsymbol{X}}_b^T \Delta \dot{\boldsymbol{X}}_b \tag{20b}$$

$$V_c = \frac{1}{2}k(\Delta X_2^2 + \Delta X_3^2) + \frac{1}{2}(\Delta \dot{X}_2^2 + \Delta \dot{X}_3^2) \triangleq \frac{k}{2}\Delta \boldsymbol{X}_c^T \Delta \boldsymbol{X}_c + \frac{1}{2}\Delta \dot{\boldsymbol{X}}_c^T \Delta \dot{\boldsymbol{X}}_c \tag{20c}$$

The subscripts (a, b, c) denote the errors of the two sides cornered at the (first, second, third) spacecraft, respectively. The final Lyapunov function candidate being controlled is chosen to be the largest sub-Lyapunov function:

$$V_{\text{ctrl}} = \max\{V_a, V_b, V_c\} \tag{21}$$

Once the control $\boldsymbol{\xi}$ is determined, the motions of the three sides are determined by Eq. (9). To develop a control algorithm to only stabilize two sides at once, the dynamics of the two sides being controlled are

$$\ddot{\boldsymbol{X}}_{\text{ctrl}} = [B_{\text{ctrl}}]\boldsymbol{\xi} + \boldsymbol{f}_{\text{ctrl}} \tag{22}$$

where $[B_{\text{ctrl}}]$ is a 2×3 matrix with the two rows selected from the matrix $[B]$ according to the two sides being controlled.

Taking a first-order time derivative of V_{ctrl}, assuming the derivative is taken not at the time of switch, yields

$$\dot{V}_{\text{ctrl}} = \Delta \dot{\boldsymbol{X}}_{\text{ctrl}}^T (k\Delta \boldsymbol{X}_{\text{ctrl}} + [B_{\text{ctrl}}]\boldsymbol{\xi} + \boldsymbol{f}_{\text{ctrl}}) \tag{23}$$

Let $\dot{V}_{\text{ctrl}}$ forced to be

$$\dot{V}_{\text{ctrl}} = -\Delta \dot{\boldsymbol{X}}_{\text{ctrl}}^T [P_2] \Delta \dot{\boldsymbol{X}}_{\text{ctrl}} \tag{24}$$

where $[P_2]$ is a 2×2 positive definite matrix. Substituting Eq. (23) into Eq. (24), yields

$$[B_{\text{ctrl}}]\boldsymbol{\xi} = -k\Delta \boldsymbol{X}_{\text{ctrl}} - \boldsymbol{f}_{ctrl} - [P_2]\Delta \dot{\boldsymbol{X}}_{\text{ctrl}} \tag{25}$$

Note that $[B_{\text{ctrl}}]$ is a 2×3 matrix. As mentioned in the beginning of this section, there is a family of solutions of $\boldsymbol{\xi}$ that satisfy the control condition in Eq. (25). Let us begin with the minimum norm solution to Eq. (25):

$$\hat{\boldsymbol{\xi}} = [B_{\text{ctrl}}]^{\dagger}(-k\Delta \boldsymbol{X}_{\text{ctrl}} - \boldsymbol{f}_{\text{ctrl}} - [P_2]\Delta \dot{\boldsymbol{X}}_{\text{ctrl}}) \tag{26}$$

where $[B_{\text{ctrl}}]^{\dagger} = [B_{\text{ctrl}}]^T([B_{\text{ctrl}}][B_{\text{ctrl}}]^T)^{-1}$ is the pseudoinverse of the matrix $[B_{\text{ctrl}}]$. Note that $\hat{\boldsymbol{\xi}}$ in Eq. (26) is the minimum solution to Eq. (25) which minimizes the norm of the $\boldsymbol{\xi}$ vector. The general solution to Eq. (25) can be written as

$$\boldsymbol{\xi} = \hat{\boldsymbol{\xi}} + \gamma \cdot \boldsymbol{b}_{\text{ctrl}} \tag{27}$$

where $\boldsymbol{b}_{\text{ctrl}}$ is a 3×1 base vector of the null space of the matrix $[B_{\text{ctrl}}]$. Because $[B_{\text{ctrl}}]$ is a 2×3 matrix, it always has a nonempty null space. The scalar parameter $\gamma \in \mathcal{R}$ can be any real number. The flexibility of the value of γ provides a single degree of freedom (DOF) that can be used to find an implementable (real spacecraft charge) control solution.

So far the implementation problem has been narrowed down to finding a proper value of γ to make the solution $\boldsymbol{\xi}$ implementable. Reiterate the implementability criterion as

$$\xi_1 \cdot \xi_2 \cdot \xi_3 \geq 0 \tag{28}$$

Substituting Eq. (27) into the criterion, yields

$$g(\gamma) \triangleq \xi_1 \cdot \xi_2 \cdot \xi_3 = (\hat{\xi}_1 + \gamma b_{\text{ctrl}}(1))(\hat{\xi}_2 + \gamma b_{\text{ctrl}}(2))(\hat{\xi}_3 + \gamma b_{\text{ctrl}}(3)) \geq 0 \tag{29}$$

where $\hat{\xi}_i$ is given by the minimum norm solution in Eq. (26). The next step is to find a value of γ that satisfies the inequality $g(\gamma) \geq 0$. Note that $g(\gamma)$ is a cubic equation of γ. The two examples of the function $g(\gamma)$ are illustrated in Fig. 3. In both cases, there are two continuous intervals of γ that make $g(\gamma) \geq 0$. Generally, even when there exist a pair of imaginary solutions, the open region (2) in the case that $b_{ctrl}(1)b_{ctrl}(2)b_{ctrl}(3) > 0$ and the open region (3) in the case that $b_{\text{ctrl}}(1)b_{\text{ctrl}}(2)b_{\text{ctrl}}(3) < 0$ still exist. This indicates that there always exists a family of solutions that make the two-side control implementable with the same dynamic behavior.

Because there is an infinite number of solutions that make the control implementable, a solution is chosen which minimizes the spacecraft charge magnitudes to simplify the technical implementation of this charge control solution, this extra DOF is used to find an optimal solution that minimizes the spacecraft charge magnitudes. A charge cost function is defined:

$$J(\gamma) = \sum_{i=1}^{3} q_i^2 \tag{30}$$

Reference [18] develops an algorithm based on Newton's method to search the optimal solution of γ that minimizes the cost function $J(\gamma)$

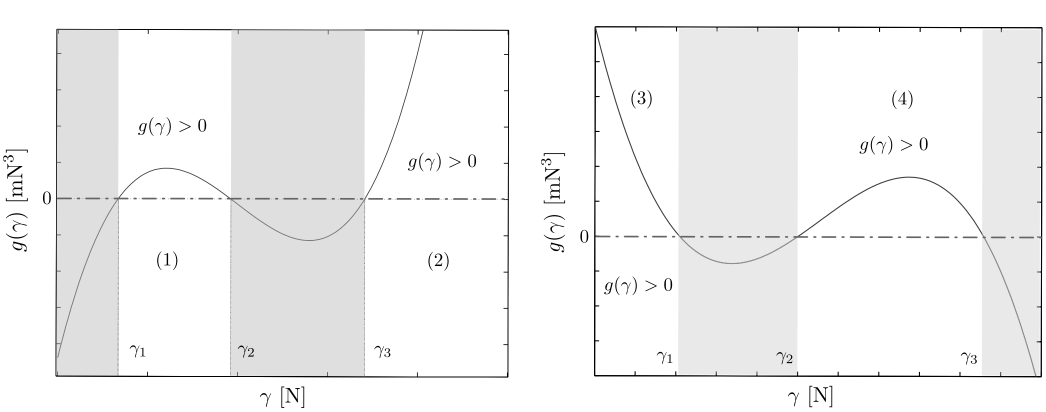

a) $\boldsymbol{b}_{\text{ctrl}}(1)\boldsymbol{b}_{\text{ctrl}}(2)\boldsymbol{b}_{\text{ctrl}}(3) > 0$ b) $\boldsymbol{b}_{\text{ctrl}}(1)\boldsymbol{b}_{\text{ctrl}}(2)\boldsymbol{b}_{\text{ctrl}}(3) < 0$

Fig. 3 Examples of $g(\gamma)$ function in two cases.

subject to the implementation requirement $g(\gamma) > 0$. The same algorithm is applied in this paper to determine the charge-optimal solution.

In the ideal case with the control being continuous, the Lyapunov function being controlled is continuous and nonincreasing. However, in praxis the control frequency is always limited resulting control cycles of finite duration. The discrete control time step makes the Lyapunov function being controlled discontinuous at the switch point. This discontinuity breaks down the stability proof based on continuous Lyapunov function. The next section uses a multiple Lyapunov function analysis tool to analyze the stability of the switched system and develops a stable switch strategy with present of the limited control time step.

IV. Multiple Lyapunov Functions Analysis

The last section designs a switching control strategy that always controls the worst two sides of the triangle, with the worst two sides defined by the corresponding Lyapunov function candidates. Stability is ensured if the switching can occur infinitely fast. The action of the switching may cause stability issues if the switching occurs over finite time steps. The tracking error of the uncontrolled triangle side can become the largest error during the finite control interval.

Multiple Lyapunov functions for switched systems is a tool to analyze this type of systems with discretely switched control objectives [19]. Before analyzing the switched system, it is necessary to define several concepts.

A *switched system* is a simple case of a hybrid system that is of multimodal, while the system switches in a way that there are finite switches in finite time [19].

A *control cycle period* is the time period while the control has to be constant without updating, it is limited by the hardware components such as sensors and actuators. The value of the control cycle period is constant.

A *switch cycle period* is the time period during when the active Lyapunov function has not been switched. The value of the switch cycle period is not constant, the minimum possible value is equal to the control cycle period.

The switched control developed in the last section switches according to the three Lyapunov functions defined in Eq. (20). Now the switch frequency is constrained by the control cycle period. The maximum switch frequency is the inverse of the control cycle period. This satisfies the definition of the switched system that there are finite switches in finite time.

A. Stability Analysis

The stability of a switched system can not be characterized using only the Lyapunov stability theorem of a continuous system. Even when all the Lyapunov function rates of the activated models are negative semidefinite, the system can still be unstable due to the control objective switching.

Figure 4 shows a simulation example of the three-body Coulomb virtual structure control using the continuous control strategy developed in the previous section, but implemented with finite control cycles. Figure 4a shows the distance errors, Figs. 4b–4d show the Lyapunov functions in different time ranges. The plots show that the system is stable during Region 1, but unstable during Region 2. Special tools should be engaged to explain and analyze this behavior.

Branicky's contribution in [19] is a milestone in analyzing nonlinear hybrid system. He proves several theorems that justify the

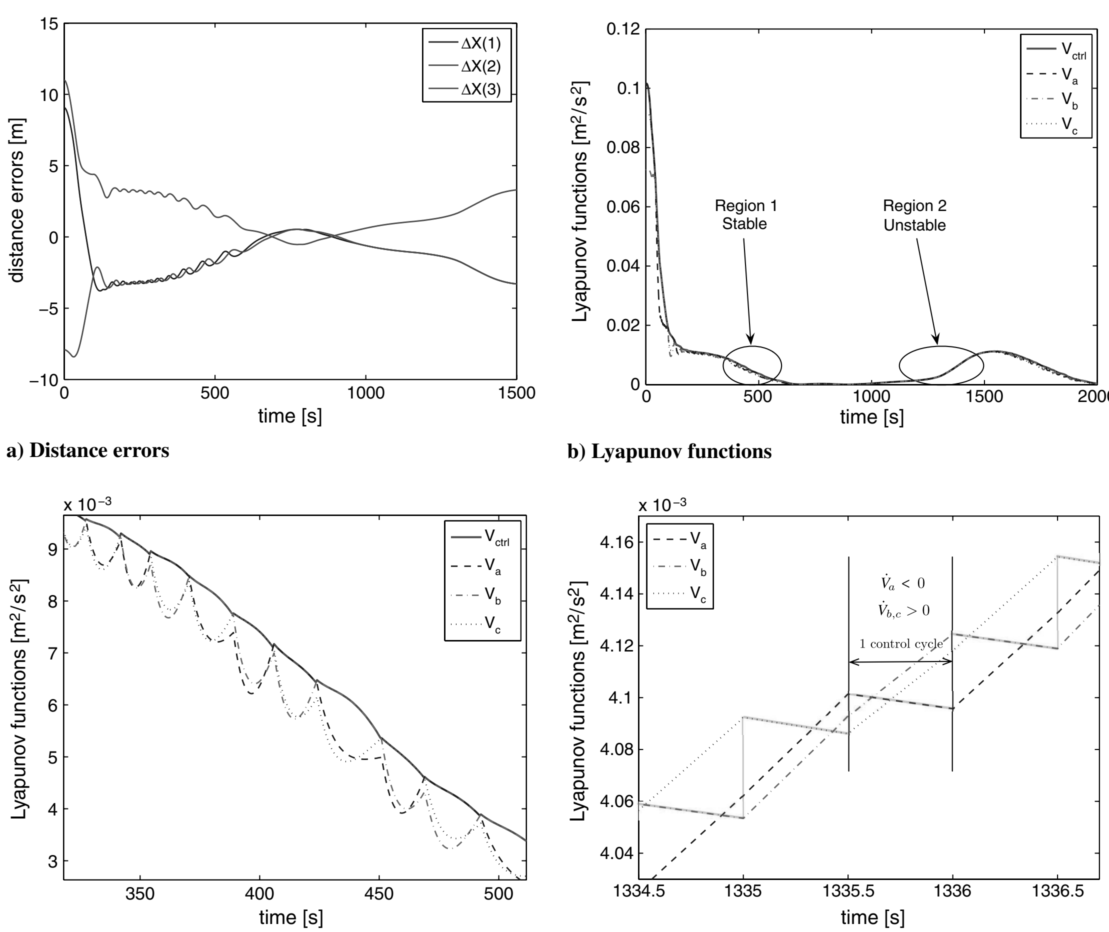

a) Distance errors

b) Lyapunov functions

c) Stable switch

d) Unstable switch

Fig. 4 Simulation example of the unstable switch control strategy.

stability of different hybrid systems based on Lyapunov's stability theorem. This paper employs Theorem 2.3 from [19] repeated here for clarity:

Theorem 2.3 [19]: Suppose we have candidate Lyapunov functions V_i, $i = 1, \cdots, N$ and vector fields $\dot{x} = f_i(x)$. Let $\mathcal{S}$ be the set of all switching sequences associated with the system.

If for each $S \in \mathcal{S}$ we have that for all i, V_i is Lyapunov-like for f_i and $x_S(\cdot)$ over $S|i$ ($S|i$ denotes the endpoints of the times that system i is active), then the system is stable in the sense of Lyapunov, where "Lyapunov-like function" is defined as:

Given a strictly increasing sequence of times T in $\mathcal{R}$, we say that V is Lyapunov-like for function f and trajectory $x(\cdot)$ over T if: 1) $\dot{V} \leq 0$ when the corresponding mode is activated and 2) V is monotonically nonincreasing on $\mathcal{E}(T)$, where $\mathcal{E}(T)$ denotes the even sequence of T: $t_0, t_2, t_4, \cdots$. □

Theorem 1 explains the behavior in Fig. 4. Figure 4c shows a snapshot at Region 1. It can be seen that at every other switching time, each Lyapunov function candidate is less than its value at the time point that is two switching cycles before. By Theorem 1, the Lyapunov function candidates (V_a, V_b, V_c) are Lyapunov-like and the system is stable in this region. Figure 4d is a snapshot during Region 2. In this case, the control switches at the maximum frequency and the switching cycle period is equal to the control cycle period. Even though during each control cycle the controlled Lyapunov function is decreasing, the uncontrolled Lyapunov functions increase faster than the controlled Lyapunov function's decreasing rate. At every other switching time, each Lyapunov function candidate is greater than its value at the time that is two switching periods earlier. So the Lyapunov function candidates (V_a, V_b, V_c) is not Lyapunov-like during Region 2, the stability is not ensured in this region.

The stability of the switched control strategy given by Eq. (21) and (27) is not guaranteed because the Lyapunov function candidates (V_a, V_b, V_c) are not guaranteed to be Lyapunov-like.

B. Switched Control Stability Requirements

Theorem 1 explains why the stability of switched control strategy given by Eq. (21) and Eq. (27) is not ensured. This section improves the control strategy to make the Lyapunov function candidates V_{a-c} satisfy the Lyapunov-like conditions, such that the system is made stable even with discrete nonzero control cycles.

Assume that during one switching cycle V_β is the controlled Lyapunov function. The corresponding two sides being controlled are denoted as ith and jth sides, the uncontrolled side is the kth side. Here "uncontrolled" does not mean the control will not affect the kth side, but the kth is not taken into consideration in developing the control algorithm. Note that when V_β is under control, the errors in the ith and jth sides are decreasing, but the trend of the error in the kth side is undetermined.

Figure 4d shows an example that when V_a is decreasing, V_b and V_c are increasing at a very high rate. This means that the errors in the L_{12} and L_{13} sides are decreasing, but the error in the L_{23} side is increasing dramatically and destroys the stability of the system. To ensure stability of the system, the uncontrolled side's behavior can not be neglected.

Note that the control in Eq. (27) makes the errors in both of the two sides ith and jth decreasing. The error in the uncontrolled side needs to be investigated. Define three error functions in the same form as the Lyapunov function candidates:

$$V_1 = \frac{k}{2}\Delta X_1^2 + \frac{1}{2}\Delta\dot{X}_1^2, \qquad V_2 = \frac{k}{2}\Delta X_2^2 + \frac{1}{2}\Delta\dot{X}_2^2$$
$$V_3 = \frac{k}{2}\Delta X_3^2 + \frac{1}{2}\Delta\dot{X}_3^2 \tag{31}$$

Without loss of generality, rearrange the state vector in the form

$$\boldsymbol{X} = \begin{pmatrix} \boldsymbol{X}_{\text{ctrl}} \\ X_{\text{uc}} \end{pmatrix} \tag{32}$$

where $\boldsymbol{X}_{\text{ctrl}}$ is composed of two distance errors corresponding to the two controlled side, X_{uc} denote the distance error of the uncontrolled side. Correspondingly the EOM is rewritten to be

$$\begin{pmatrix} \ddot{\boldsymbol{X}}_{\text{ctrl}} \\ \ddot{X}_{\text{uc}} \end{pmatrix} = \begin{bmatrix} [B_{\text{ctrl}}] \\ \boldsymbol{B}_{\text{uc}} \end{bmatrix} (\hat{\boldsymbol{\xi}} + \gamma \boldsymbol{b}_{\text{ctrl}}) + \begin{pmatrix} \boldsymbol{f}_{\text{ctrl}} \\ f_{\text{uc}} \end{pmatrix} \tag{33}$$

where $\boldsymbol{B}_{\text{uc}}$ is a 1×3 vector that is the line in the matrix $[B]$ corresponding to the uncontrolled side, f_{uc} is the component of the vector $\boldsymbol{f}$ corresponding to the uncontrolled side. Substituting $\hat{\boldsymbol{\xi}}$ in Eq. (26) into Eq. (33) and carrying out the algebra, yields

$$\begin{pmatrix} \ddot{\boldsymbol{X}}_{\text{ctrl}} \\ \ddot{X}_{\text{uc}} \end{pmatrix} = \begin{pmatrix} -k\Delta\boldsymbol{X}_{\text{ctrl}} - [P_2]\Delta\dot{\boldsymbol{X}}_{\text{ctrl}} \\ \boldsymbol{B}_{\text{uc}}[B_{\text{ctrl}}]^{\dagger}(-k\Delta\boldsymbol{X}_{\text{ctrl}} - [P_2]\Delta\dot{\boldsymbol{X}}_{\text{ctrl}} - \boldsymbol{f}_{\text{ctrl}}) + \gamma\boldsymbol{B}_{\text{uc}}\boldsymbol{b}_{\text{ctrl}} + f_{\text{uc}} \end{pmatrix} \tag{34}$$

Taking a time derivative of the error function of the uncontrolled side V_{uc} and substituting $\ddot{X}_{\text{uc}}$, yield

$$\begin{aligned} \dot{V}_{\text{uc}} &= k\Delta\dot{X}_{\text{uc}}(\Delta X_{\text{uc}} + \Delta\ddot{X}_{\text{uc}}) \\ &= k\Delta\dot{X}_{\text{uc}}(\Delta X_{\text{uc}} + \boldsymbol{B}_{\text{uc}}[B_{\text{ctrl}}]^{\dagger}(-k\Delta\boldsymbol{X}_{\text{ctrl}} - [P_2]\Delta\dot{\boldsymbol{X}}_{\text{ctrl}} - \boldsymbol{f}_{\text{ctrl}}) \\ &\quad + \gamma\boldsymbol{B}_{\text{uc}}\boldsymbol{b}_{\text{ctrl}} + f_{\text{uc}}) \end{aligned} \tag{35}$$

Equation (35) shows that the sign of the uncontrolled side's error is undetermined. Even though there are two parameters $[P_2]$ and γ that can be adjusted, this flexibility does not guarantee there exists a solution to make $\dot{V}_{\text{uc}}$ negative because in some cases controlling three sides is impossible.

To find a way to solve this problem, it is beneficial to take a closer look at the unstable situation shown in Fig. 4d. Note that the three Lyapunov function candidates are actually the combinations of the error functions:

$$V_a = V_1 + V_3, \qquad V_b = V_1 + V_2, \qquad V_c = V_2 + V_3 \tag{36}$$

Figure 5 shows the details of the Lyapunov function candidates and the error functions during several unstable switches. In Fig. 5a, during the nth switch cycle, $\dot{V}_c < 0$ while $\dot{V}_a$ and $\dot{V}_b$ are positive. $\dot{V}_c < 0$ indicates $\dot{V}_2 < 0$ and $\dot{V}_3 < 0$. This is verified by Fig. 5b. So $V_{a,b} > 0$ is due to the excessive increasing of V_1, as shown in Fig. 5b. At the beginning of the next control cycle, $(n+1)$th control cycle, it is identified that V_a is the largest Lypunov function candidate. According to the switch strategy in Eq. (21), the controller switches to control V_a which indicates $V_{1,3} < 0$ as shown in Fig. 5b. Focusing on V_1 in Fig. 5b, one can see that during the $(n+1)$th control cycle, V_1 is controlled such that $\dot{V}_1 < 0$. But the rate of decreasing of V_1 is smaller than its increasing rate during the nth control cycle. This results in that at the next switch time (at the point C in Fig. 5b), V_1 has not decreased to the same level as the value at the beginning of the nth control cycle (at the point A). That is $V_1^{(C)} > V_1^{(A)}$. According to Branicky's theorem in Theorem 1, V_1 is not Lyapunov-like and the stability is not guaranteed.

By the above analysis, it can be concluded that the instability comes from two sources:

1) The decreasing rate of the error function of the new controlled side is not big enough to compensate for its increased amount during the last control cycle.

2) The new, uncontrolled error function is growing too fast.

Upon entering a new control objective switch, both the new uncontrolled and the new controlled sides' error functions need to be taken care of to ensure the Lyapunov function candidates to be Lyapunov-like. Corresponding to Fig. 5b, the magnitude of the slope of V_1 during the $(n+1)$th control cycle should be greater than the slope during the nth control cycle. The increasing rate of V_2 during the $(m+1)$th control cycle should be less than its decreasing rate during the nth control cycle. Figure 6 illustrates this idea. In this way,

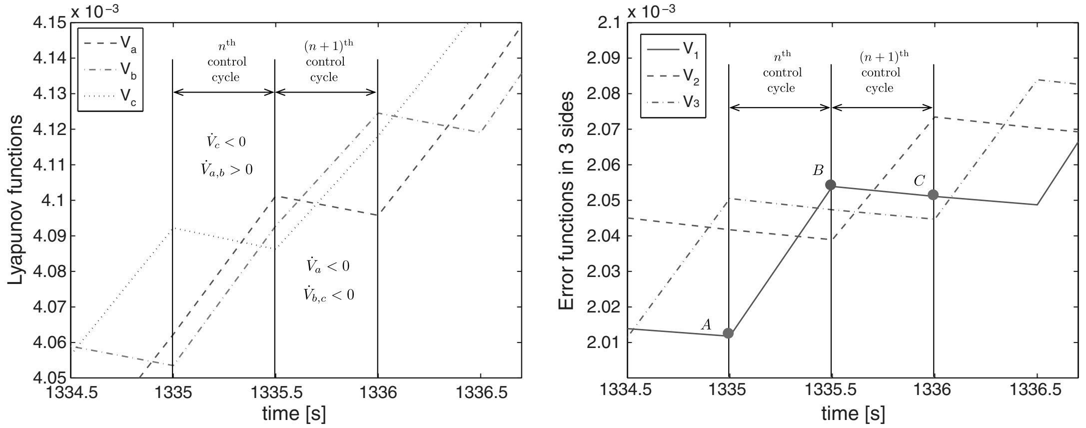

a) Lyapunov function candidates

b) Error functions

Fig. 5 Unstable switch analysis.

$V_1^{(C)} < V_1^{(A)}$ and $V_2^{(C)} < V_2^{(A)}$. V_3 is always being controlled during the two control cycles so it is automatically satisfied that $V_3^{(c)} < V_3^{(A)}$. Thus all of the Lyapunov function candidates are Lyapunov-like during the two control cycles.

To take care of the new controlled side, which indicates this side was uncontrolled over possibly several control cycles, the first step is to determine the requirement to remain Lyapunov-like for this side. Let V_m denote the new controlled side's error function. The requirement for this side to be Lyapunov-like is that the change of the corresponding error function in the new switch cycle $\Delta V_m^{(n+1)}$ should be less than its change in the previous switch cycle $\Delta V_m^{(n)}$. This can be expressed mathematically:

$$\int_{(n+1)} \dot{V}_m^{(n+1)}\, \mathrm{d}t < -\Delta V_m^{(n)} \tag{37}$$

where $\int_{(n+1)}$ means the integration across the $(n+1)$th switch cycle. Because the control cycle period is very small, the inequality in Eq. (37) is approximated by

$$\dot{V}_m^{(n+1)} \Delta t < -\Delta V_m^{(n)} \tag{38}$$

where Δt is the control cycle period which is constant. This requires the error function rate $\dot{V}_m^{(n+1)}$ should be less than a certain value:

$$\dot{V}_m^{(n+1)} < -\Delta V_m^{(n)}/\Delta t \tag{39}$$

Because the subscript m denotes the new controlled side, $\dot{V}_m^{(n+1)}$ is determined to be negative. If $\Delta V_m^{(n)}$ is negative which means V_m decreases in the nth control cycle, then the requirement in Eq. (39) is automatically satisfied. Otherwise, a strategy that makes the inequality in Eq. (41) always satisfied is expected. Taking a time derivative of V_m then substituting the EOM of X_m in Eq. (33) yields

$$\dot{V}_m = \Delta\dot{X}_m(k\Delta X_m + \boldsymbol{B}_m[B_{\mathrm{ctrl}}]^{\dagger} \times (-k\Delta\boldsymbol{X}_{\mathrm{ctrl}} - [P_2]\Delta\dot{\boldsymbol{X}}_{\mathrm{ctrl}} - \boldsymbol{f}_{\mathrm{ctrl}}) + \boldsymbol{f}_m) \tag{40}$$

In this expression of $\dot{V}_m$ only the control coefficients k and $[P_2]$ are not dependent on the states and can be used to adjust the value of $\dot{V}_m$. This paper choose to change the matrix $[P_2]$ to make the error functions to be Lyapunov-like. Substituting Eq. (40) into the inequality in Eq. (41), yields

$$\Delta\dot{X}_m\boldsymbol{B}_m[B_{\mathrm{ctrl}}]^{\dagger}[P_2]\Delta\dot{\boldsymbol{X}}_{\mathrm{ctrl}} > \Delta\dot{X}_m(k\Delta X_m + f_m + \boldsymbol{B}_m[B_{\mathrm{ctrl}}]^{\dagger}(-k\Delta\boldsymbol{X}_{\mathrm{ctrl}} - \boldsymbol{f}_{\mathrm{ctrl}})) + \frac{\Delta V_m^{(n)}}{\Delta t} \tag{41}$$

The inequality in Eq. (41) is the requirement for the matrix $[P_2]$ that ensures the error function of the new controlled side is Lyapunov-like. The requirement for the new uncontrolled side is similar:

$$\Delta\dot{X}_{\mathrm{uc}}\boldsymbol{B}_{\mathrm{uc}}[B_{\mathrm{ctrl}}]^{\dagger}[P_2]\Delta\dot{\boldsymbol{X}}_{\mathrm{ctrl}} > \Delta\dot{X}_{\mathrm{uc}}(k\Delta X_{\mathrm{uc}} + f_{\mathrm{uc}} + \boldsymbol{B}_{\mathrm{uc}}[B_{\mathrm{ctrl}}]^{\dagger}(-k\Delta\boldsymbol{X}_{\mathrm{ctrl}} - \boldsymbol{f}_{\mathrm{ctrl}})) + \frac{\Delta V_{\mathrm{uc}}^{(n)}}{\Delta t} \tag{42}$$

The inequalities in Eqs. (41) and (42) are two conditions that guarantees the error functions to be Lyapunov-like. Note that the matrix $[P_2]$ should be positive definite, so there are three requirements for $[P_2]$ that ensures a globally stable switched control.

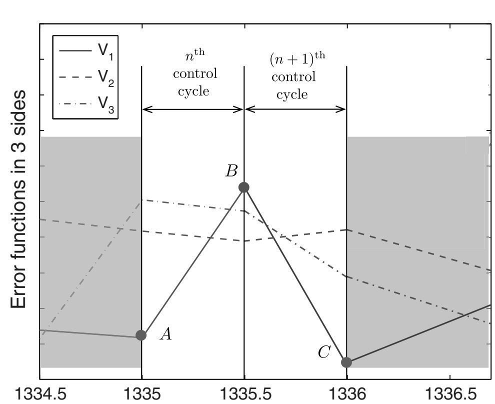

Fig. 6 Hand-drawn illustration of the new switch strategy effect.

C. Stable Switched Strategy

The previous section determined three requirements that ensured a stable switched control. This section develops a new switched control strategy that implements the stability requirements found in Eqs. (41) and (42). Above all, the existence of solutions that satisfy the stability requirements needs to be investigated. Let us begin with introducing an asymmetric positive definite matrix.

Property 1: A 2×2 matrix $[A]$ in the form

$$[A] = \begin{bmatrix} A_{11} & A_{12} \\ -A_{12} & A_{22} \end{bmatrix} \tag{43}$$

is a positive definite matrix if and only if

$$A_{11} > 0, \qquad A_{22} > 0 \tag{44}$$

Proof: The symmetric part of the matrix $[A]$ is

$$[A_s] = \frac{1}{2}[A] + \frac{1}{2}[A]^T = \begin{bmatrix} A_{11} & 0 \\ 0 & A_{22} \end{bmatrix} \tag{45}$$

It is evident that the symmetric matrix $[A_s]$ is positive definite if and only if $A_{11} > 0$ and $A_{22} > 0$. A necessary and sufficient condition for a real matrix to be positive definite is that its symmetric part is positive definite. Thus the matrix $[A]$ is positive definite if and only if $A_{11} > 0$ and $A_{22} > 0$. □

This form of a positive definite matrix is more general than symmetric positive definite matrices. This provides more flexibility in solving the inequalities in Eqs. (41) and (42). Note that the inequalities in Eqs. (41) and (42) can be written in the general form

$$\boldsymbol{a}^T[P_2]\boldsymbol{b} > c \tag{46}$$

where $\boldsymbol{a}$ and $\boldsymbol{b}$ are two two-dimensional vectors, c is a real number that equals the right hand side of the inequalities. The following theorem studies the existence of the solutions to this inequality.

Theorem 2: Assume a positive definite matrix in the form

$$[A] = \begin{bmatrix} A_{11} & A_{12} \\ -A_{12} & A_{22} \end{bmatrix} \tag{47}$$

where A_{11} and A_{22} are positive. Define two arrays: $\boldsymbol{a} = [a_1, a_2]^T$ and $\boldsymbol{b} = [b_1, b_2]^T$. If the following two inequalities and one equation do not happen at the same time

$$a_1 b_1 < 0 \tag{48a}$$

$$a_2 b_2 < 0 \tag{48b}$$

$$a_2 b_1 = a_1 b_2 \tag{48c}$$

then for any $c \in \mathbb{R}$, there always exists a solution of the matrix $[A]$ that satisfies the inequality

$$\boldsymbol{a}^T[A]\boldsymbol{b} > c \tag{49}$$

Proof: It needs to be proved that the solution of $[A]$ exists under the following two cases: 1) $a_2 b_1 \neq a_1 b_2$ and 2) $a_2 b_1 = a_1 b_2$ and $a_1 b_1 > 0$ and/or $a_2 b_2 > 0$.

Carrying out the algebra in the inequality in Eq. (47), yields

$$a_1 b_1 A_{11} + (a_1 b_2 - a_2 b_1) A_{12} + a_2 b_2 A_{22} > c \tag{50}$$

Note that the requirements for A_{ij} are $A_{11} > 0$ and $A_{22} > 0$, the third element A_{12} can be any real number. Next the existence of the positive definite matrix $[A]$ is proven under the enumerated two cases.

Case 1: $a_2 b_1 \neq a_1 b_2$. When $a_2 b_1 \neq a_1 b_2$, the element A_{12} can be used to adjust the value of the left hand side of the inequality in Eq. (50). If $a_1 b_2 > a_2 b_1$, then any real value of A_{12} that satisfies

$$A_{12} > \frac{c - a_1 b_1 A_{11} - a_2 b_2 A_{22}}{a_1 b_2 - a_2 b_1} \tag{51}$$

is a solution to the inequality in Eq. (47) while preserving the positive definiteness of the matrix $[A]$. Alternatively if $a_1 b_2 < a_2 b_1$, then any real value of A_{12} that satisfies

$$A_{12} < \frac{c - a_1 b_1 A_{11} - a_2 b_2 A_{22}}{a_1 b_2 - a_2 b_1} \tag{52}$$

is a solution to the inequality in Eq. (47).

Case 2: $a_2 b_1 = a_1 b_2$ and $a_1 b_1 > 0$ and/or $a_2 b_2 > 0$. When $a_2 b_1 = a_1 b_2$, the inequality in Eq. (50) simplifies to

$$a_1 b_1 A_{11} + a_2 b_2 A_{22} > c \tag{53}$$

Because either $a_1 b_1 > 0$ or $a_2 b_2 > 0$, without loss of generality it is supposed $a_1 b_1 > 0$. Solving for A_{11} from the inequality in Eq. (53), yields

$$A_{11} > \frac{1}{a_1 b_1}(c - a_2 b_2 A_{22}) \tag{54}$$

The inequality in Eq. (54) does not conflict with the requirement that $A_{11} > 0$. Thus any value of A_{11} that satisfies

$$A_{11} > \max\left\{\frac{1}{a_1 b_1}(c - a_2 b_2 A_{22}), 0\right\} \tag{55}$$

is a solution to the inequality in Eq. (47). □

Theorem 2 proves the existence of solutions to the inequalities in Eqs. (41) and (42) unless the condition in Eq. (48) occurs. Note that the two inequalities and one equation in Eq. (48) are rarely to happen at the same time. By intuition without rigorous proof, here it is assumed that $a_1 b_2 = a_2 b_1$ is a transient state. The situation given by Eq. (48) is never detected in simulations.

So far all the preparations are in place to present the stable switched control strategy. Note that the previous switch strategy shown in Eq. (21) works well most of the time. The temporary loss of stability happens is due to the discrete control time steps which result in violation of the Lyapunov-like condition. The previous switch strategy given by Eq. (21) is still valid unless the Lyapunov-like condition is violated.

Beginning a new control cycle, there are three possible combinations of the controlled sides. One of them corresponds to no switching case, the other two correspond to two switched control cases. For notational convenience, denote the three possibilities as *no switching*, *switch-1* and *switch-2*. When an unstable switching, which means the switching does not satisfy the requirements in Eqs. (41) and (42), is detected, it is easier to change the new controlled side than to change the value of the matrix $[P_2]$. Upon this situation, at first the controller switches the sides being controlled without changing the value of $[P_2]$. If simply switching sides can not ensure Lyapunov-like condition, the controller changes the matrix $[P_2]$.

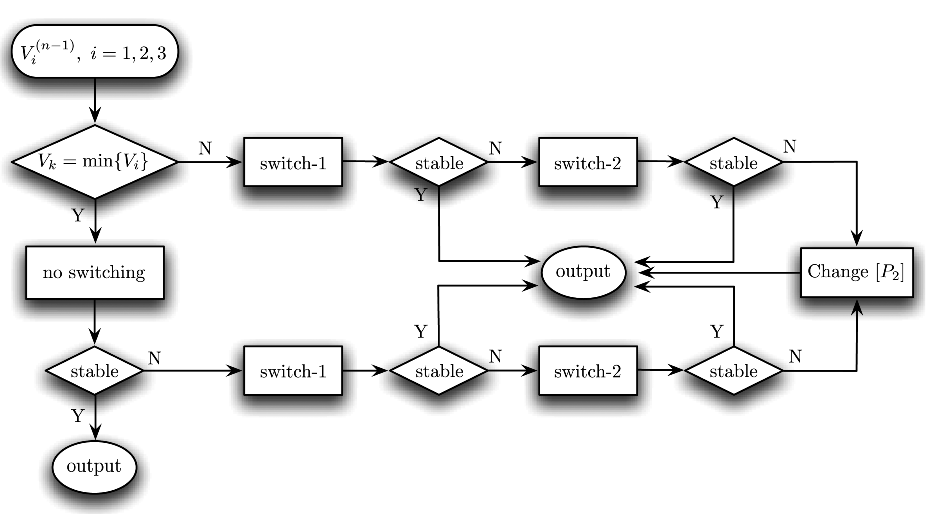

Fig. 7 Stable switch strategy flow chart.

Figure 7 illustrates the strategy of switching. The details of calculating the value of the matrix $[P_2]$ is not illustrated. Upon changing the value of $[P_2]$, it is better to start with simpler diagonal form. If the diagonal form of $[P_2]$ matrix cannot provide a stable switched control, then the more complex asymmetric matrix form as shown in Eq. (47) is sought. The proof of Theorem 2 provides requirement of $[P_2]$ that ensures stability. To summarize, one element of $[P_2]$ (either $P_2(1,1)$ or $P_2(1,2)$, denote it as $P_{2,c}$) must be greater than or less than a certain value (denote the value as p_s). To implement this requirement, a coefficient τ is introduced to define an equality constraint:

$$P_{2,c} = \tau p_s \tag{56}$$

When $P_{2,c}$ should be greater than p_s, $\tau > 1$ is chosen; when $P_{2,c}$ should be less than p_s, $\tau < 1$ is chosen.

V. Numerical Simulations

This section presents numerical simulations to show the effectiveness and performance of the stable switched three-craft charge control. The desired shape here is triangular configuration. For notational convenience, the old controller with the switching strategy given by Eq. (21) is called Controller-1, the new stable controller with the switching strategy given by Fig. 7 is called Controller-2.

Both Controller-1 and Controller-2 are used to control the three-craft Coulomb virtual structure. Under the same initial conditions the performances of the two controllers can be compared. The Controller-1 has different unstable behavior when the control charge level is different. The following numerical simulations demonstrate the behaviors of the control in two cases: large control effort case and small control effort case. The response of the system is different in different situations. When the initial errors and separation distances

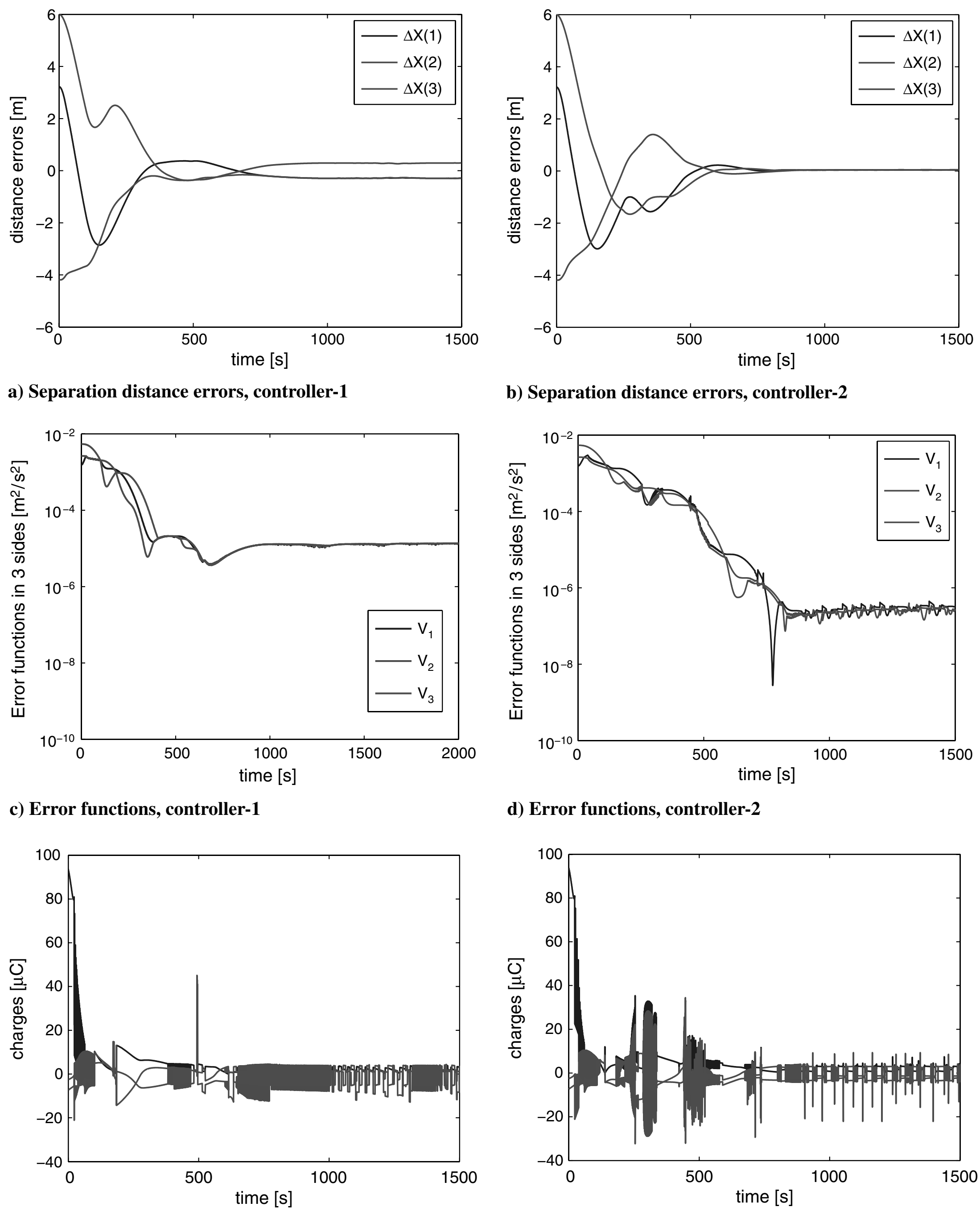

a) Separation distance errors, controller-1

b) Separation distance errors, controller-2

c) Error functions, controller-1

d) Error functions, controller-2

e) Charges, controller-1

f) Charges, controller-2

Fig. 8 Big control effort simulations.

are large, the control charges levels are large. The following two simulation cases illustrate the behavior of the system under two controllers. In all of the simulations the masses of the three spacecraft are the same:

$$m_1 = m_2 = m_3 = 50 \text{ kg} \tag{57}$$

A. Large Control Effort Case

The initial positions and velocities of the three spacecraft are

$$\begin{cases} \boldsymbol{r}_1 = [9, -2, 0]^T \text{ m} \\ \boldsymbol{r}_2 = [0, -4, 0]^T \text{ m} \\ \boldsymbol{r}_3 = [-2, -2, 0]^T \text{ m} \end{cases}, \quad \begin{cases} \dot{\boldsymbol{r}}_1 = [0, 0.01, 0]^T \text{ m/s} \\ \dot{\boldsymbol{r}}_2 = [0, 0, 0]^T \text{ m/s} \\ \dot{\boldsymbol{r}}_3 = [0, -0.01, 0]^T \text{ m/s} \end{cases} \tag{58}$$

The expected triangular shape of the virtual structure is defined by the separation distances:

$$\boldsymbol{X}^* = [6, 7, 5]^T \text{ m} \tag{59}$$

The proportional feedback coefficients are

$$k = 0.0003 \text{ s}^{-2} \tag{60}$$

The nominal value of the matrix $[P_2]$ is

$$[P_2^*] = \begin{bmatrix} 0.02 & 0 \\ 0 & 0.02 \end{bmatrix} \text{ s}^{-1} \tag{61}$$

Note that the value of the $[P_2]$ matrix is varying using Controller-2.

Figure 8 shows the responses of the system under the two different control strategy. Comparing the separation distance errors in Figs. 8a and 8b, it is evident that the stable switched control strategy performs better than the unstable switched control. Using this set of initial

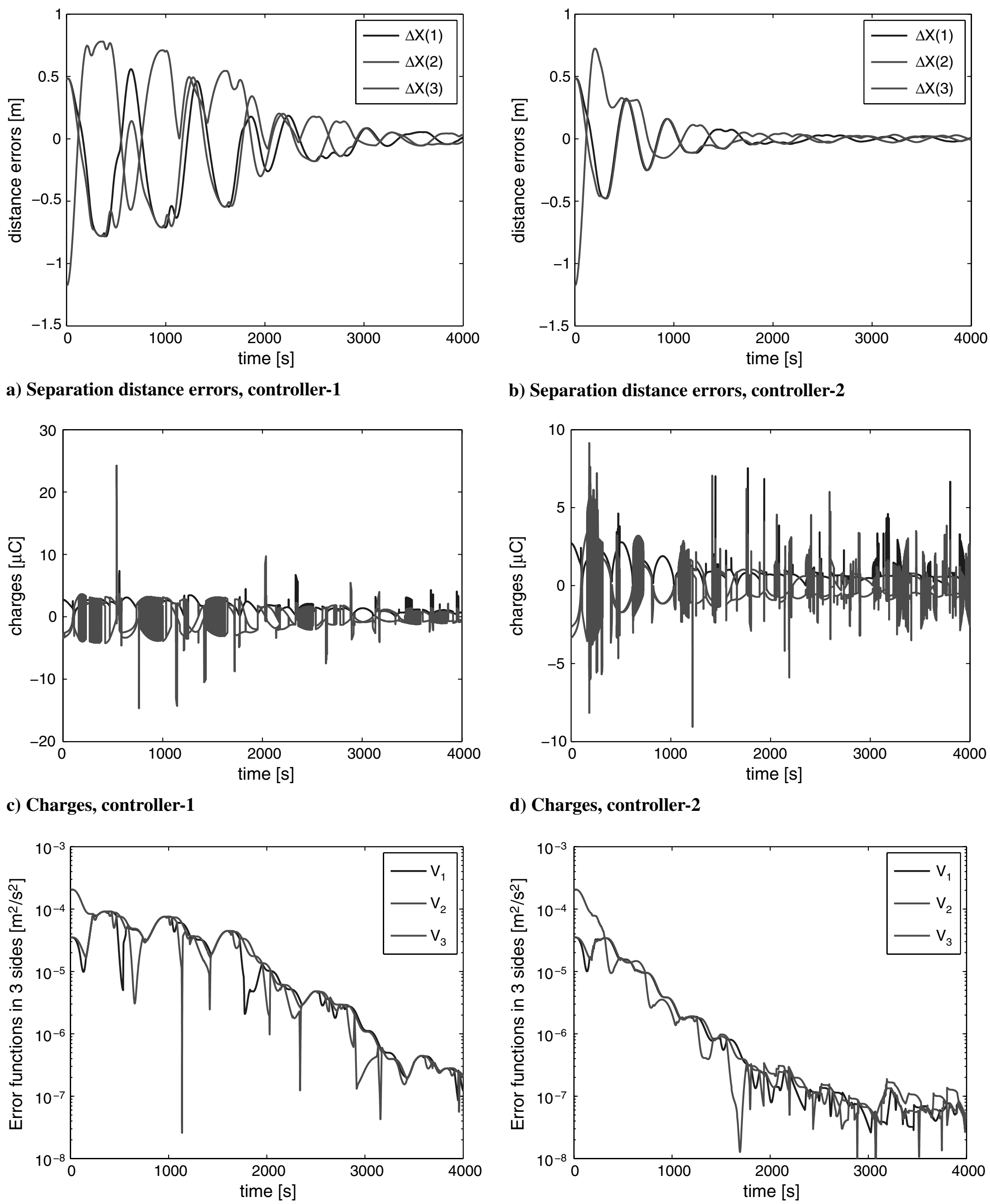

a) Separation distance errors, controller-1

b) Separation distance errors, controller-2

c) Charges, controller-1

d) Charges, controller-2

e) Error functions, controller-1

f) Error functions, controller-2

Fig. 9 Small control effort simulations.

states and controller parameters, the old controller assuming continuos switching capabilities cannot stabilize the distance errors to zero, while the stable switched control strategy with finite control cycles stabilizes the errors near zero. Because the rotating triangular configuration is not an equilibrium solutions, the errors cannot converge perfectly to zero. The smaller the control cycles are, the smaller the final state errors will become.

The error functions' histories in Fig. 8c explains the behavior of the continuous-switching controller. During the time around 700–1000 s, the controller switches at the highest frequency and the error functions do not satisfy the Lyapunov-like conditions. The details are similar to Fig. 5b. The error histories in Fig. 8a indicate this region is an unstable segment. Figure 8d shows that under the control of the stable switched control strategy, the error functions drop to very low level (10^{-7} m^2/s) within 1000 s, but will not really decrease to zero. This means the system is stable, but not asymptotically stable as explained above.

Figures 8e and 8f show the charge histories of the two simulations. It can be seen that under the control of the stable switched controller, the charge histories have more spikes than that of the unstable switched control. This is due to the variation of the matrix $[P_2]$ in the stable switched control. Despite the spikes in the charge histories, it can be seen that after the distance errors settle down (after 800 s as shown in Fig. 8b), the control charge level that holds the spinning triangle is around 5 μC. But at the beginning the charge level goes up to 90 μC, which is challenging to practically implement. This simulation case is aggressive. The intention of this simulation case is to demonstrate different behaviors under different situations.

B. Small Control Effort Case

In this simulation, the initial errors and the separation distances are small thus the controllers require small charge levels. The initial conditions are set as

$$\begin{cases} \boldsymbol{r}_1 = [2, 0, 0] \text{ m} \\ \boldsymbol{r}_2 = [0, -4, 0] \text{ m} \\ \boldsymbol{r}_3 = [-2, -2, 0] \text{ m} \end{cases}, \quad \begin{cases} \dot{\boldsymbol{r}}_1 = [0, 0.002, 0] \text{ m/s} \\ \dot{\boldsymbol{r}}_2 = [0, 0, 0] \text{ m/s} \\ \dot{\boldsymbol{r}}_3 = [0, -0.002, 0] \text{ m/s} \end{cases} \tag{62}$$

The expected separation distances are given by

$$\boldsymbol{X}^* = [4, , 4, 4]^T \text{ m} \tag{63}$$

The controller coefficients are

$$k = 0.0003 \text{ s}^{-2}, \qquad [P_2^*] = \text{diag}(0.005, 0.005) \text{ s}^{-1} \tag{64}$$

Figure 9 shows the simulation results under the two controllers. Figures 9a, 9c, and 9e show the results of the simulation using Controller-1. The distance error history in Fig. 9a shows that at the beginning 2000 s, the errors are staying at high level. The error functions shown in Fig. 9e verify that during [0, 2000] s, there are several temporary unstable regions where both of the three error functions are increasing. After 2000 s, the distance errors are decreasing significantly.

Figures 9b, 9d, and 9f show the results of the simulation using Controller-2. Figure 9b shows that the distance errors decrease and stabilize to zero in much shorter time than using Controller-1. Comparing the charge histories in Figs. 9c and 9d, it can be seen that there are more spikes when Controller-2 is being used. Figure 9b also shows that the distance errors do not converge to zero. This is because the new switched control Controller-2 is stable, but not asymptotically stable.

It is not always the case that Controller-2 performs better than Controller-1. Under different initial conditions and different controller coefficients Controller-1 may perform better than Controller-2. There is one difference between the two simulation cases. When using Controller-1 in the large control effort case in the illustrated simulation results, the distance errors settles down to a certain level and stack there. But in the small control effort case, the distance errors keep changing and will not stay at a certain level.

VI. Conclusions

This paper studies a three-spacecraft Coulomb formation triangular shape control problem. Assuming continuous-switching capability, a two-side switched control strategy is developed to always control the worst two sides instead of controlling both of the three sides. Here an implementable control solution is always guaranteed. However, the discrete control time steps may cause temporary instability of the shape control. A stable switched control strategy is developed based on the multiple Lyapunov functions analysis. This new switch strategy ensures all of the error functions to be Lyapunov-like thus stability is guaranteed. Numerical simulations demonstrate the improvement of the stable switched control. The new switched control also induces spikes in the control charges because the new control changes the value of the distance rate feedback gain matrix to ensure stability. The method of employing Lyapunov-like control functions is a promising approach to investigate the relative control of charged spacecraft with more than three vehicles. The new switched control strategy is successful in stabilizing a nonequilibrium triangular shape. Further research will investigate how this control can be used to control three-craft collinear equilibrium shapes.

References

[1] Ren, W., and Beard, R. W., "Virtual Structure Based Spacecraft Formation Control with Formation Feedback," AIAA Guidance, Navigation and Control Conference and Exhibit, Monterey, CA, 5–8 Aug. 2002.

[2] King, L. B., Parker, G. G., Deshmukh, S., and Chong, J.-H., "Spacecraft Formation-Flying Using Inter-Vehicle Coulomb Forces," NASA/NIAC, TR, Jan. 2002, http://www. niac.usra.edu.

[3] Berryman, J., and Schaub, H., "Static Equilibrium Configurations in GEO Coulomb Spacecraft Formations," 15th AAS/AIAA Space Flight Mechanics Meeting, 23–27 Jan. 2005.

[4] Berryman, J., and Schaub, H., "Analytical Charge Analysis for 2- and 3-Craft Coulomb Formations," *Journal of Guidance, Control, and Dynamics*, Vol. 30, Nov.–Dec. 2007, pp. 1701–1710. doi:10.2514/1.23785

[5] Schaub, H., Hall, C., and Berryman, J., "Necessary Conditions for Circularly-Restricted Static Coulomb Formations," *Journal of the Astronautical Sciences*, Vol. 54, Nos. 3–4, July–Dec. 2006, pp. 525–541.

[6] Vasavada, H., and Schaub, H., "Analytic Solutions for Equal Mass Four-Craft Static Coulomb Formation," *Journal of the Astronautical Sciences*, Vol. 56, No. 1, Jan.–March 2008, pp. 7–40.

[7] Natarajan, A., sand Schaub, H., "Linear Dynamics and Stability Analysis of a Coulomb Tether Formation," *Journal of Guidance, Control, and Dynamics*, Vol. 29, July–Aug. 2006, pp. 831–839. doi:10.2514/1.16480

[8] Natarajan, A., and Schaub, H., "Hybrid Control of Orbit Normal and Along-Track Two-Craft Coulomb Tethers," *Aerospace Science and Technology*, Vol. 13, June–July 2009, pp. 183–191. doi:10.1016/j.ast.2008.10.002

[9] Natarajan, A., Schaub, H., and Parker, G. G., "Reconfiguration of a Nadir-Pointing 2-Craft Coulomb Tether," *Journal of British Interplanetary Society*, Vol. 60, Nos. 4–5, June 2007, pp. 209–218.

[10] Natarajan, A., and Schaub, H., "Orbit-Nadir Aligned Coulomb Tether Reconfiguration Analysis," AAS/AIAA Spaceflight Mechanics Meeting, AAS Paper 08-149, Galveston, TX, 27–31 Jan. 2008.

[11] Lappas, V., Saaj, C., Richie, D., Peck, M., Streeman, B., and Schaub, H., "Spacecraft Formation Flying and Reconfiguration with Electrostatic Forces," AAS/AIAA Space Flight Mechanics Meeting, Sedona, AZ, AAS Paper 07–113, 28 Jan.–1 Feb. 2007.

[12] Wang, S., and Schaub, H., "Spacecraft Collision Avoidance Using Coulomb Forces with Separation Distance and Rate Feedback," *Journal of Guidance, Control, and Dynamics*, Vol. 31, May–June 2008, pp. 740–750. doi:10.2514/1.29634

[13] Wang, S., and Schaub, H., "Open-Loop Electrostatic Spacecraft Collision Avoidance Using Patched Conics Analysis," AAS/AIAA Spaceflight Mechanics Meeting, Galveston, TX, AAS Paper 08-207, 27–31 Jan. 2008.

[14] Wang, S., and Schaub, H., "Electrostatic Spacecraft Collision Avoidance Using Piece-Wise Constant Charges," AAS/AIAA Space Flight Mechanics Meeting, AAS Paper 09-184, Savannah, GA, 8–12 Feb. 2009.

[15] Hussein, I. I., and Schaub, H., “Invariant Shape Solutions of the Spinning Three Craft Coulomb Tether Problem,” *Celestial Mechanics and Dynamical Astronomy*, Vol. 96, Oct. 2006, pp. 137–157. doi:10.1007/s10569-006-9043-8

[16] Schaub, H., and Hussein, I. I., “Stability and Reconfiguration Analysis of a Circulary Spinning 2-Craft Coulomb Tether,” IEEE Aerospace Conference, Big Sky, MT, 3–10 March 2007.

[17] Hussein, I. I., and Schaub, H., “Stability and Control of Relative Equilibria for the Three-Spacecraft Coulomb Tether Problem,” *Acta Astronautica*, Vol. 65, Nos. 5–6, 2009, pp. 738–754. doi:10.1016/j.actaastro.2009.03.035

[18] Wang, S., and Schaub, H., “1-D Constrained Coulomb Structure Stabilization with Charge Saturation,” AAS/AIAA Astrodynamics Specialists Conference, AAS Paper 07–267, Mackinac Island, MI, 19–23 Aug. 2007.

[19] Branicky, M. S., “Multiple Lyapunov Functions and Other Analysis Tools for Switched and Hybrid Systems,” *IEEE Transactions on Automatic Control*, Vol. 43, April 1998, pp. 475–482. doi:10.1109/9.664150